Phosphorylation of the Mdm2 oncoprotein by the c-Abl tyrosine kinase regulates p53 tumor suppression and the radiosensitivity of mice

Michael I. Carr[a], Justine E. Roderick[b], Hong Zhang[a], Bruce A. Woda[c], Michelle A. Kelliher[b], and Stephen N. Jones[a,b,1]

[a]Department of Cell and Developmental Biology, University of Massachusetts Medical School, Worcester, MA 01655; [b]Department of Molecular, Cell, and Cancer Biology, University of Massachusetts Medical School, Worcester, MA 01655; and [c]Department of Pathology, University of Massachusetts Medical School, Worcester, MA 01655

Edited by Carol Prives, Columbia University, New York, NY, and approved November 15, 2016 (received for review July 21, 2016)

The p53 tumor suppressor acts as a guardian of the genome by preventing the propagation of DNA damage-induced breaks and mutations to subsequent generations of cells. We have previously shown that phosphorylation of the Mdm2 oncoprotein at Ser394 by the ATM kinase is required for robust p53 stabilization and activation in cells treated with ionizing radiation, and that loss of Mdm2 Ser394 phosphorylation leads to spontaneous tumorigenesis and radioresistance in *Mdm2*^{S394A} mice. Previous in vitro data indicate that the c-Abl kinase phosphorylates Mdm2 at the neighboring residue (Tyr393) in response to DNA damage to regulate p53-dependent apoptosis. In this present study, we have generated an Mdm2 mutant mouse (*Mdm2*^{Y393F}) to determine whether c-Abl phosphorylation of Mdm2 regulates the p53-mediated DNA damage response or p53 tumor suppression in vivo. The *Mdm2*^{Y393F} mice develop accelerated spontaneous and oncogene-induced tumors, yet display no defects in p53 stabilization and activity following acute genotoxic stress. Although apoptosis is unaltered in these mice, they recover more rapidly from radiation-induced bone marrow ablation and are more resistant to whole-body radiation-induced lethality. These data reveal an in vivo role for c-Abl phosphorylation of Mdm2 in regulation of p53 tumor suppression and bone marrow failure. However, c-Abl phosphorylation of Mdm2 Tyr393 appears to play a lesser role in governing Mdm2-p53 signaling than ATM phosphorylation of Mdm2 Ser394. Furthermore, the effects of these phosphorylation events on p53 regulation are not additive, as *Mdm2*$^{Y393F/S394A}$ mice and Mdm2^{S394A} mice display similar phenotypes.

c-Abl | Mdm2 | DNA damage | p53 | tumorigenesis

The significant role of p53 in human tumor suppression is evidenced by the fact that p53 is either mutated or functionally inactive in over 50% of human cancers (1). The tumor suppressive activity of p53 has been classically attributed to p53-dependent cellular responses of growth arrest and apoptosis in response to various stresses, although increasing evidence has implicated additional p53-target genes involved in regulating further cellular processes such as metabolic functions and DNA repair (2, 3). Stress-induced p53 responses are preceded by a profound increase in p53 protein levels and transcriptional activity. Accordingly, understanding the signaling events that lead to p53 stabilization and transcriptional activation has been the focus of extensive research. In order for p53 levels and activity to increase in the damaged cell, p53 must be relieved of the negative regulation imposed by the MDM oncoproteins, Mdm2 and MdmX.

Regulation of the DNA damage response (DDR) in mammals is governed by the PI3K-related ATM and ATR kinases. Activation of these transducer kinases depends on the type and amount of DNA damage and triggers the direct or indirect phosphorylation of numerous downstream proteins involved in the DDR (4, 5). ATM is activated primarily by double-strand breaks (DSBs), and its numerous target substrates include p53, Mdm2, and MdmX (6–10). We have previously reported the generation of a mouse model (*Mdm2*^{S394A}) in which ATM phosphorylation of Mdm2 at serine residue 394 (Ser395 in human MDM2) was abolished (11). Cells and tissues of *Mdm2*^{S394A} mice display profound defects in DNA damage-induced p53 protein stabilization and transcriptional activation. The diminished p53 response in these animals resulted in reduced p53-dependent apoptosis in hematopoietic tissues, radioresistance, and increased spontaneous tumorigenesis. These findings underscore that Mdm2 phosphorylation is a critical event in regulating Mdm2-p53 signaling and the induction of p53 activity during the DDR and in homeostatic tissues. However, *Mdm2*^{S394A} mice display some p53 stabilization and activity following DNA damage and do not fully phenocopy *p53*$^{-/-}$ mice. This led us to examine whether the phosphorylation of additional Mdm2 residues contributes to p53 induction following DNA damage.

Intriguingly, the tyrosine residue immediately preceding Ser395 in human MDM2, Tyr394 (Tyr393 in mouse Mdm2), has been shown to be phosphorylated by the tyrosine kinase c-Abl (12, 13). Similar to ATM and ATR, c-Abl is activated by a variety of DNA damaging agents (14–16). Previous overexpression studies in cell lines indicate that c-Abl promotes growth arrest in a p53-dependent manner and apoptosis by both p53-dependent and independent mechanisms (17, 18). Furthermore, c-Abl can protect p53 from MDM2-mediated degradation, and c-Abl phosphorylation of MDM2 overcomes the inhibitory effect of MDM2 on p53 transcriptional activity and apoptosis (19). In addition, studies using *c-abl*$^{-/-}$ mouse embryonic fibroblasts (MEFs) indicate that c-Abl is required for maximal p53 accumulation in response to ionizing radiation (IR), doxorubicin, or mitomycin C treatment, and that

Significance

The p53 transcription factor is stabilized in response to cellular stress and regulates the expression of genes involved in numerous biological activities, thereby suppressing tumorigenesis. DNA damage and other stress signals upregulate p53, in part, by freeing p53 from negative regulation imposed by the Mdm2 and MdmX (Mdm4) oncoproteins. MDM proteins are subject to posttranslational modification, and accumulating evidence indicates that phosphorylation of Mdm2 by different stress-activated kinases such as ATM or c-Abl alters Mdm2-p53 signaling and profoundly affects p53 function. A better understanding of the in vivo effects of Mdm2 phosphorylation may facilitate the development of novel therapeutics capable of stimulating p53 antitumor activity or alleviating p53-dependent toxicities in nonmalignant tissues.

Author contributions: M.I.C. and S.N.J. designed research; M.I.C. and J.E.R. performed research; J.E.R. and M.A.K. contributed new reagents/analytic tools; M.I.C., J.E.R., H.Z., B.A.W., M.A.K., and S.N.J. analyzed data; and M.I.C. and S.N.J. wrote the paper.

The authors declare no conflict of interest.

This article is a PNAS Direct Submission.

[1]To whom correspondence should be addressed. Email: stephen.jones@umassmed.edu.

This article contains supporting information online at www.pnas.org/lookup/suppl/doi:10.1073/pnas.1611798114/-/DCSupplemental.

coexpression of c-Abl overcomes MDM2-mediated ubiquitination and nuclear export of p53 (20). c-Abl phosphorylates MDM2 Tyr394 as well as Tyr276 and Tyr405 (12, 13), and c-Abl phosphorylation of MDM2 Tyr394 impairs the ability of MDM2 to inhibit p53 stabilization and transactivation and p53-mediated apoptosis (12). More recently, it was proposed that c-Abl phosphorylation of MDM2 increases MDM2–MDMX binding and promotes MDM2-directed MDMX ubiquitination, and that this ultimately destabilizes the MDM2–MDMX complex, promoting p53 stabilization (21).

As we have shown that ATM phosphorylation of Mdm2 Ser394 profoundly impacts the p53 response to DNA damage in mice, we sought to determine whether c-Abl phosphorylation of Mdm2 Tyr393 similarly regulates p53 functions in vivo. To this end, we generated a knockin mouse model in which Mdm2 Tyr393 is substituted with phenylalanine ($Mdm2^{Y393F}$), as well as a mouse in which both the c-Abl target residue Mdm2 Tyr393 and the adjacent ATM target residue Mdm2 Ser394 are mutated ($Mdm2^{Y393F/S394A}$), enabling the study of whether phosphorylation of these residues has additive or redundant effects.

Results

***$Mdm2^{Y393F}$* Mice Are Viable and Display Increased Spontaneous and Oncogene-Induced Tumorigenesis.** To investigate the role of Mdm2 Tyr393 phosphorylation under physiological conditions, we generated a mouse model in which this tyrosine residue is substituted with a phenylalanine residue (Y393F). Site-directed mutagenesis was performed to introduce an A-to-T missense mutation in the 393 codon, and a synonymous G-to-C mutation in the 397 codon of *Mdm2* exon 12 (Fig. 1*A*). A gene-replacement vector was constructed to replace the endogenous *Mdm2* exon 12 sequences with the mutated exon 12 (Fig. S1*A*). Gene targeting was performed in PC3 (129SV) embryonic stem (ES) cells (22), and homologous recombination was confirmed in G418-resistant clones by Southern blotting (Fig. S1 *A*–*C*). Blastocyst injection of targeted ES clones produced several high-degree male chimeras that passed the Mdm2 *Y393F* allele through their germ line. Southern blotting further confirmed proper targeting in F1 and F2 generation mice, along with protamine-Cre–directed deletion of the floxed neomycin cassette (Fig. S1 *D* and *E*). The presence of the additional synonymous G-to-C mutation within the 397 codon of the targeted allele introduced a novel BtsCI restriction digest site that allowed for identification of the $Mdm2^{Y393F}$ allele by PCR-digest strategy (Fig. 1*A* and Fig. S1*F*). *Mdm2* transcripts from spleens of $Mdm2^{Y393F}$ mice were sequenced and confirmed as containing only the targeted mutations (Fig. 1*A*). Heterozygous intercrosses yielded homozygous $Mdm2^{Y393F}$ mice at Mendelian ratios, indicating that $Mdm2^{Y393F}$ is not compromised in its function during development (Fig. S1*G*). Additionally, no differences were observed in average litter size, body weights at 6 wk of age, or male-to-female sex distribution.

We have previously shown that mice deficient for phosphorylation of the neighboring residue (Mdm2 Ser394) by ATM are prone to spontaneous tumorigenesis (11). Therefore, we sought to examine whether c-Abl phosphorylation of Mdm2 Tyr393 impacted tumor suppression. Cohorts of WT and $Mdm2^{Y393F}$ mice were established and monitored for tumor formation. During the 24-mo tumor assay, 8 of 21 (38%) $Mdm2^{Y393F}$ mice developed spontaneous tumors (Fig. 1*B*), whereas only 1 of 28 (4%) WT mice presented with a tumor at 20 mo of age. $Mdm2^{Y393F}$ tumors arose between 14.5 and 24 mo of age, a similar latency as seen in $Mdm2^{S394A}$ mice (11). The majority of tumors arose in lymphatic tissues, and 5 of the 6 tumors (83%) were identified as B-cell lymphomas, with one of the B-cell lymphomas also containing atypical T cells. Other tumor types seen in the cohort included a myeloid sarcoma, a hepatocellular carcinoma, and a papillary tumor of lacrimal origin (Fig. 1 *C*–*E*).

As $Mdm2^{Y393F}$ mice were more prone to develop spontaneous tumors of lymphoid origin, we further examined the effects of Mdm2-Y393 phosphorylation on tumor suppression using the *Eμ-Myc* mouse model (23). Cohorts of *Eμ-Myc* and *Eμ-Myc;* $Mdm2^{Y393F}$ mice were generated (C57BL/6 background) and assayed for tumor formation. *Eμ-Myc* mice develop pre-B/B-cell lymphomas within 3–6 mo of age, and we observed a median time to tumorigenesis of 125.5 d in the *Eμ-Myc* model cohort (Fig. 1*F*), a duration in close agreement with previous studies (23, 24). However, *Eμ-Myc;*$Mdm2^{Y393F}$ mice displayed significantly accelerated tumorigenesis, with a median time to tumor formation of only 76.5 d. Thus, whereas dispensable for development, c-Abl phosphorylation of Mdm2-Y393 significantly impacts tumorigenesis by preventing the formation of both spontaneous and oncogene-induced tumors.

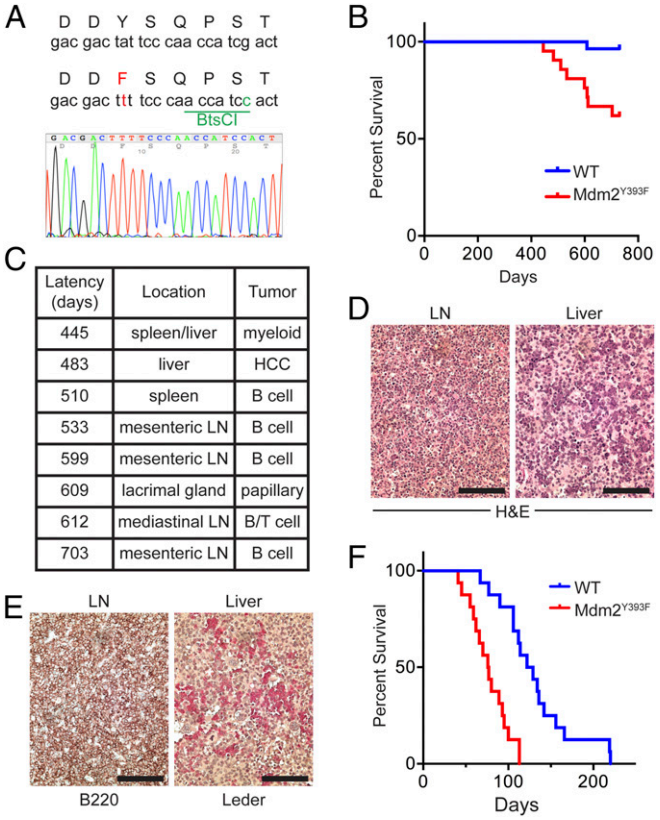

Fig. 1. $Mdm2^{Y393F}$ mice are viable and display increased spontaneous and oncogene-induced tumorigenesis. (*A*) DNA sequence of WT and $Mdm2^{Y393F}$ allele surrounding codon 393 (*Top*). An A-to-T mutation changed codon 393 from Tyr to Phe. A silent G-to-C mutation in codon 397 introduced a BtsCI restriction site. Sequencing results of the corresponding region from $Mdm2^{Y393F}$ spleen cDNA are shown (*Bottom*). (*B*) Kaplan–Meier tumor-free survival curves of WT ($n = 28$) and $Mdm2^{Y393F}$ ($n = 21$) mice. Curves were compared by log-rank test: ($P < 0.01$). (*C*) Table displaying the latency, location, and tumor type for spontaneous tumors arising in $Mdm2^{Y393F}$ mice. LN, lymph node; HCC, hepatocellular carcinoma. (*D*) Representative H&E-stained tissue sections of a LN exhibiting a B-cell lymphoma (*Left*) and myeloid sarcoma present in the liver sinusoids (*Right*). (Scale bars, 100 μm.) (*E*) The B-cell lymphomas show expression of B220 (*Left*), and the myeloid neoplasms exhibit chloroacetate esterase (Leder) staining (*Right*). (Scale bars, 100 μm.) (*F*) Kaplan–Meier tumor-free survival curves of *Eμ-Myc* ($n = 16$) and *Eμ-Myc;*$Mdm2^{Y393F}$ ($n = 16$) mice. Median survival times were as follows: *Eμ-Myc* (125.5 d), *Eμ-Myc;* $Mdm2^{Y393F}$ (76.5 d). Curves were compared by log-rank test ($P < 0.0001$).

c-Abl Phosphorylation of Mdm2 Tyr393 Does Not Influence DNA Damage-Induced p53 Stabilization and Activation in Spleen and Thymus. Having observed increased lymphomagenesis in $Mdm2^{Y393F}$ mice, and as c-Abl is activated by a variety of DNA damaging agents (14–16), we next examined whether c-Abl phosphorylation of Mdm2 Tyr393 impacts DNA damage-induced p53 stabilization and activation in lymphatic tissues of $Mdm2^{Y393F}$ mice. WT and

CELL BIOLOGY

Mdm2^{Y393F} mice were exposed to 5 Gy IR and spleens were analyzed for p53 and Mdm2 levels by immunoblotting (Fig. 2*A*). In both genotypes, c-Abl cleavage was observed in response to IR, similar to previous observations in cells undergoing stress-induced apoptosis (25, 26). c-Abl phosphorylation at Tyr245 confirmed kinase activation. No qualitative differences were detected in basal or IR-induced p53 protein levels. Similarly, no obvious differences were observed in p53 activation as indicated by levels of p53-Ser18 phosphorylation. No differences were observed in the levels of Mdm2 protein, which increased at 2–4 h following IR, before decreasing as p53 activity diminished, similar to what has previously been reported in this tissue (11, 27). The lack of a difference in p53 stabilization was confirmed quantitatively in biological triplicates at 0, 2, and 4 h (Fig. S2*A*). Similar results were observed in thymi from these same animals, with no qualitative differences detected in the levels of total p53, phosphorylated p53 (S18), or Mdm2, save for slightly higher basal Mdm2 levels in *Mdm2*^{Y393F} mice (Fig. S2*B*). Consistent with equal levels of basal and IR-induced p53 protein stabilization and phosphorylation, real-time quantitative PCR (RT-qPCR) performed on cDNA from untreated and irradiated spleens of WT and *Mdm2*^{Y393F} mice detected no differences in the basal or DNA damage-induced expression levels of a selection of p53-target genes involved in growth arrest, apoptosis, DNA repair, or metabolic regulation (Fig. 2*B*). Similar results were observed in thymi (Fig. S2*C*).

Hematopoietic organs are highly radiosensitive, and p53 activation in these tissues triggers widespread apoptosis following IR (28). In keeping with the absence of observable differences in p53 stabilization and activation in *Mdm2*^{Y393F} spleens and thymi, we detected no differences in splenic or thymic apoptosis in untreated and irradiated *Mdm2*^{Y393F} mice by TUNEL (Fig. 2*C* and Fig. S2*D*). This observation was confirmed quantitatively by flow cytometry of Annexin V-FITC–stained splenocytes and thymocytes (Fig. S2 *E* and *F*). Thus, the IR-induced stabilization and activation of p53 and the resultant apoptotic response is unaltered in *Mdm2*^{Y393F} spleens and thymi.

We also examined whether Mdm2 Tyr393 phosphorylation affected p53-dependent growth arrest. MEFs from WT, *Mdm2*^{Y393F}, and *p53*$^{-/-}$ mice were untreated or exposed to either 5 Gy IR or 150 nM doxorubicin for 18 h. Flow cytometric cell-cycle analysis revealed no differences in growth arrest in *Mdm2*^{Y393F} MEFs following either irradiation or treatment with doxorubicin (Fig. S2*G*). Furthermore, WT and *Mdm2*^{Y393F} MEFs exhibited similar growth rates in standard cell proliferation assays (Fig. S2*H*).

***Mdm2*^{Y393F} Mice Are Radioresistant and Display Enhanced Bone Marrow Repopulating Abilities Following IR Exposure.** The proposed effects of c-Abl phosphorylation of Mdm2 on p53 are similar to those of ATM phosphorylation of Mdm2, namely p53 stabilization and activation. Conversely, our findings that DNA damage-induced p53 stabilization and activation in spleen and thymus, and p53-dependent apoptosis and growth arrest in *Mdm2*^{Y393F} tissues and cells, are unaltered contrasts with what we have reported with *Mdm2*^{S394A} mice. Thus, c-Abl's phosphorylation of Mdm2-Y393 may either have limited effect on the p53-dependent DDR or may be adequately compensated for by ATM phosphorylation of Mdm2 Ser394. However, when we challenged cohorts of WT and *Mdm2*^{Y393F} mice to a series of IR doses spanning the threshold-lethal range, we observed a significant resistance to whole-body IR-induced lethality in *Mdm2*^{Y393F} mice (Fig. 3*A*). Following treatment with 8 Gy IR, 74% of *Mdm2*^{Y393F} mice survived to 4 wk compared with 22% survival of WT mice. Similarly, 29% of *Mdm2*^{Y393F} mice survived to 4 wk after exposure to 9 Gy IR compared with 7% of WT mice. All mice survived 7 Gy IR for both genotypes, whereas no mice of either genotype survived past 2 wk following 10 Gy IR. The majority of mice succumbed between 1 and 3 wk post-IR. Lethality in mice treated with this range of IR doses is routinely attributed to p53-dependent bone marrow failure, referred to as "hematopoietic syndrome" (29). As we have described a similar resistance to whole-body IR in *Mdm2*^{S394A} mice (11), we next compared the effects of IR on bone marrow from WT, *Mdm2*^{Y393F}, *Mdm2*^{S394A}, and *p53*$^{-/-}$ mice. Expression of p53-target genes *Puma* and *p21* are unaltered in *Mdm2*^{Y393F} bone marrow, in agreement with what was observed in irradiated spleen and thymus (Fig. S3*A*). Conversely, expression levels of those same target genes are significantly reduced in *Mdm2*^{S394A} bone marrow, in keeping with the previously described reduced IR-induced p53 responses in these animals (11). However, similar initial reductions in bone marrow cellularity were observed in both mutants, as well as in WT mice and in *p53*$^{-/-}$ mice following treatment with 5 Gy IR (Fig. 3*B*). Thus, the initial reduction in gross cellularity appears, to some extent, to be independent of p53. Flow cytometry analysis of untreated bone marrow from WT, *Mdm2*^{Y393F}, *Mdm2*^{S394A}, and *p53*$^{-/-}$ mice revealed no differences in the populations of lineage-defined, mature hematopoietic cells, save for statistically fewer Cd11b^{+} cells in *p53*$^{-/-}$ mice (Fig. S3*B*). In agreement with the observed reduction in bone marrow cellularity in all genotypes, IR treatment induced a cumulative decline in populations of mature cells in bone marrow from each genotype (Fig. S3*C*).

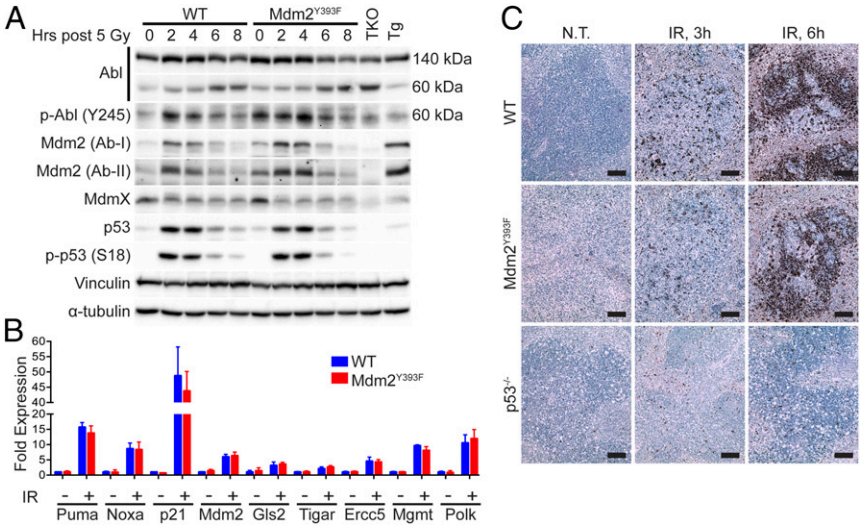

Fig. 2. c-Abl phosphorylation of Mdm2 Tyr393 does not influence DNA damage-induced p53 stabilization and activation in spleen and thymus. (*A*) WT and *Mdm2*^{Y393F} mice were left untreated or exposed to 5 Gy IR and spleens were harvested at 2-h intervals. Protein levels were analyzed by Western blotting. TKO indicates *Mdm2*$^{-/-}$, *MdmX*$^{-/-}$, *p53*$^{-/-}$ triple knockout control; Tg indicates *Mdm2*$^{Tg/+}$ Mdm2 overexpressing control. (*B*) Mice were left untreated or exposed to 5 Gy IR and spleens were harvested at 4 h. Fold expression of p53-target genes was determined by RT-qPCR, relative to untreated WT samples using *Rplp0* as internal reference (n = 3–4, ± SEM). Significance was determined by Student's t test of ΔΔCt values. (*C*) TUNEL staining of spleens of mice treated as in *A* and harvested at 3 and 6 h.

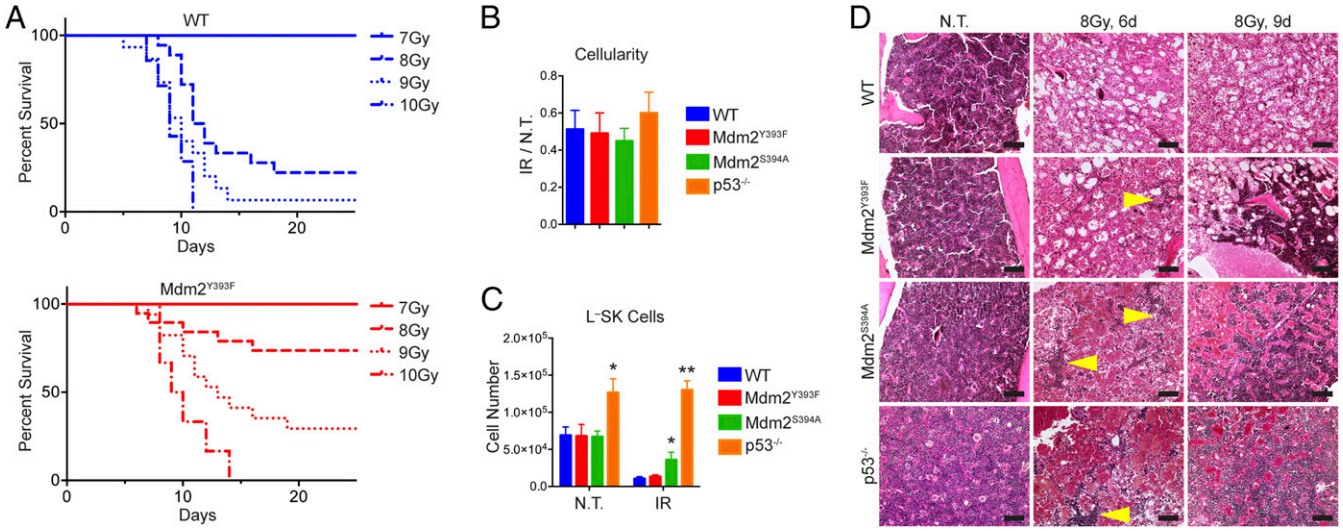

Fig. 3. *Mdm2*^{Y393F} mice are radioresistant and display improved bone marrow repopulation following IR exposure. (*A*) Kaplan–Meier survival curves of WT (n = 7–18) and *Mdm2*^{Y393F} (n = 6–19) mice exposed to 7, 8, 9, and 10 Gy whole-body IR. WT and *Mdm2*^{Y393F} curves were compared by log-rank test: 7 Gy (n.s.), 8 Gy (P = 0.003), 9 Gy (P = 0.030), and 10 Gy (n.s.). (*B*) Quantification of numbers of nucleated cells in bone marrow from both hindlimbs of WT, *Mdm2*^{Y393F}, *Mdm2*^{S394A}, and *p53*$^{-/-}$ mice either untreated or 8 h after exposure to 5 Gy IR. (n = 3–6, ± SEM). *P < 0.05, **P < 0.01 (Student's t tests). (*C*) Quantification of L$^-$SK HSPCs in bone marrow of WT, *Mdm2*^{Y393F}, *Mdm2*^{S394A}, and *p53*$^{-/-}$ mice treated as described in *B*. *P < 0.05, **P < 0.01 (Student's t tests). (*D*) H&E stained bone marrow from WT, *Mdm2*^{Y393F}, *Mdm2*^{S394A}, and *p53*$^{-/-}$ mice exposed to 8 Gy IR. Yellow arrows indicate nascent hematopoietic cell colonies. (Scale bars, 100 μm.)

Only *p53*$^{-/-}$ mice displayed significantly more B220$^+$ cells. Again, no differences were observed in the absence of treatment, in the more primitive Lin$^-$Sca1$^-$cKit$^+$ (L$^-$S$^-$K) progenitor populations of WT, *Mdm2*^{Y393F}, *Mdm2*^{S394A}, or *p53*$^{-/-}$ mice (Fig. S3*D*). However, whereas L$^-$S$^-$K cell numbers decreased 70–80% in WT, *Mdm2*^{Y393F}, and *Mdm2*^{S394A} bone marrows, bone marrow from *p53*$^{-/-}$ mice retained significantly more L$^-$S$^-$K cells following IR. This finding suggests that increased survival of hematopoietic progenitors underlies the resistance to IR-induced bone marrow failure in mice with compromised p53. Indeed, when Lin$^-$Sca1$^+$cKit$^+$ (L$^-$SK) hematopoietic stem and progenitor cells (HSPCs) were quantified in these same animals, we observed no decrease following irradiation in *p53*$^{-/-}$ mice (Fig. 3*C*). Whereas greater numbers of HSPCs were observed in untreated *p53*$^{-/-}$ mice, no differences were observed in HSPC number in untreated WT, *Mdm2*^{Y393F}, and *Mdm2*^{S394A} mice. However, there were significantly more HSPCs in *Mdm2*^{S394A} bone marrow following IR, and HSPC levels also appeared slightly (although not statistically) elevated in irradiated *Mdm2*^{Y393F} bone marrow. We examined whether the resistance to acute whole-body IR-associated lethality observed in *Mdm2*^{Y393F} and *Mdm2*^{S394A} mice was due to an increased capacity to repopulate irradiated marrow by performing H&E stains on bone marrow from mice either untreated or 6 and 9 d following 8 Gy IR (Fig. 3*D*). At 6 d post-IR, whereas mice of all three genotypes displayed evidence of a significant decrease in cellularity, both *p53*$^{-/-}$and *Mdm2*^{S394A} bone marrow, and to a lesser extent *Mdm2*^{Y393F} bone marrow, contained multiple colonies of hematopoietic cells that were not apparent in WT bone marrow, as well as visibly more erythrocytes. By 9 d post-IR, coinciding with the period of observed morbidity in threshold-lethally irradiated animals, an even larger discrepancy in cellularity was observable between WT and mutant bone marrows. Few hematopoietic colonies were visible in WT marrow, whereas colonies present in *p53*$^{-/-}$and *Mdm2*^{S394A} mice had expanded significantly and largely replenished the medullary cavity. Whereas there was greater visible repopulation in *Mdm2*^{Y393F} bone marrow compared with WT, this repopulation appeared intermediate to that observed in *Mdm2*^{S394A} bone marrow, trending with the observed improved HSPC survival following IR.

Mdm2 Tyr393 and Ser394 Phosphorylations Are Not Additive in Their Impact on Tumor Suppression and Radioresistance. To determine whether the shared effects of Mdm2 Tyr393 and Ser394 phosphorylation were redundant or additive, we generated a knockin mouse in which both the Tyr393 residue is substituted with a phenylalanine residue (Y393F) and the Ser394 residue is substituted with an alanine (S394A) (Fig. 4*A*). Gene targeting was carried out following a similar strategy as used for *Mdm2*^{Y393F} mice (Fig. S4 *A*–*E*). The targeting construct coded for an A-to-T missense mutation in the 393 codon, a T-to-G missense mutation in the 394 codon, and a synonymous T-to-G mutation in the 398 codon of *Mdm2* exon 12, which also facilitated PCR-digest genotyping of cells and mice. As observed for *Mdm2*^{S394A} mice (11), *Mdm2*$^{Y393F/S394A}$ mice were recovered from heterozygous intercrosses at Mendelian ratios (Fig. S4*F*). A cohort of biallelic *Mdm2*$^{Y393F/S394A}$ mice was monitored for spontaneous tumor presentation, and by 24 mo, 14 of 21 (67%) of these mice presented with tumors (Fig. 4*B*). This result mirrors the 65% of *Mdm2*^{S394A} mice that developed spontaneous tumors in our previous study (11), as does the observed latency of 18–24 mo for the majority of tumors. Consequently, the tumor suppressive effects of Mdm2 Tyr393 phosphorylation by c-Abl and Mdm2 Ser394 phosphorylation by ATM do not appear to be additive or synergistic. The predominant tumor type in *Mdm2*$^{Y393F/S394A}$ mice was B-cell lymphoma (6/15, 40%), along with myeloid sarcomas (5/15, 33%), hepatocellular carcinomas (3/15, 20%), and one tumor that appeared to be a liver metastasis of neuroendocrine cell origin (Fig. 4 *C*–*E*).

Irradiated thymi from *Mdm2*$^{Y393F/S394A}$ mice were examined by immunoblotting, as well as by qPCR of p53-target gene transcripts, and showed a similar reduction of p53 stabilization and activity as observed in *Mdm2*^{S394A} mice (Fig. S5 *A* and *B*). This finding is in keeping with the absence of observable defects in the p53 response to DNA damage in *Mdm2*^{Y393F} mice described in Fig. 2 and Fig. S2. Accordingly, whereas reduced in comparison with WT, no additional deficits in apoptosis were observed by TUNEL staining or Annexin V

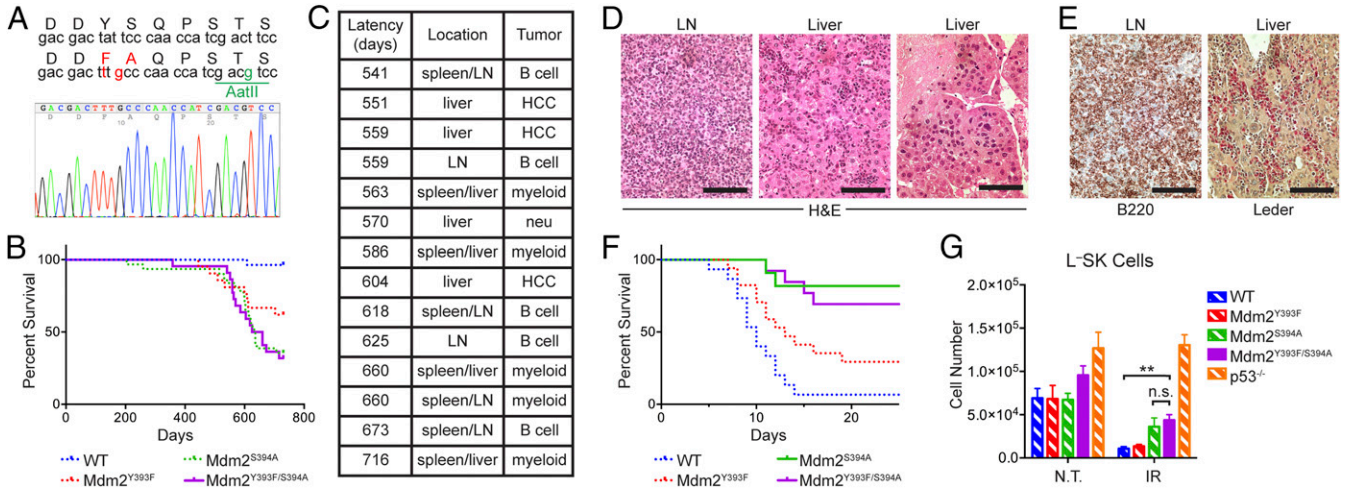

Fig. 4. Mdm2 Tyr393 and Ser394 phosphorylations are not additive in their impact on tumor suppression or radioresistance. (*A*) DNA sequence of WT and $Mdm2^{Y393F/S394A}$ allele surrounding codons 393 and 394 (*Top*). An A-to-T mutation changed codon 393 from Tyr to Phe. A T-to-C mutation changed codon 394 from Ser to Ala. A silent T-to-G mutation in codon 398 introduced a AatII restriction site. Sequencing results of the corresponding region from $Mdm2^{Y393F/S394A}$ spleen cDNA are shown (*Bottom*). (*B*) Kaplan–Meier tumor-free survival curve of $Mdm2^{Y393F/S394A}$ mice ($n = 21$). Included are tumor-free survival curves of WT and $Mdm2^{Y393F}$ mice described in Fig. 1*B* and $Mdm2^{S394A}$ mice described previously (11). Curves were compared by log-rank test: $Mdm2^{Y393F/S394A}$ to WT ($P < 0.0001$) and $Mdm2^{Y393F/S394A}$ to $Mdm2^{Y393F}$ ($P = 0.080$). (*C*) Table displaying the latency, location, and tumor type for spontaneous tumors arising in $Mdm2^{Y393F/S394A}$ mice. LN, lymph node; HCC, hepatocellular carcinoma; Neu, neuroendocrine. (*D*) Representative H&E-stained tissue sections of a B-cell lymphoma (*Left*), myeloid sarcoma (*Middle*), and hepatoma (*Right*) that developed in $Mdm2^{Y393F/S394A}$ mice. (Scale bars, 100 μm.) (*E*) B-cell lymphoma shows expression of B220 (*Left*), and a myeloid neoplasm exhibits chloroacetate esterase (Leder) activity (*Right*). (Scale bars, 100 μm.) (*F*) Kaplan–Meier survival curves of WT ($n = 15$), $Mdm2^{Y393F}$ ($n = 17$), $Mdm2^{S394A}$ ($n = 11$), and $Mdm2^{Y393F/S394A}$ ($n = 13$) mice exposed to 9 Gy whole-body IR. Curves were compared by log-rank test: WT to $Mdm2^{Y393F}$ ($P = 0.030$), WT to $Mdm2^{S394A}$ ($P < 0.0001$), WT to $Mdm2^{Y393F/S394A}$ ($P < 0.0001$), $Mdm2^{Y393F}$ to $Mdm2^{S394A}$ ($P = 0.010$), $Mdm2^{Y393F}$ to $Mdm2^{Y393F/S394A}$ ($P = 0.020$), and $Mdm2^{S394A}$ to $Mdm2^{Y393F/S394A}$ (n.s.). (*G*) Quantification of L^-SK HSPCs in bone marrow of WT, $Mdm2^{Y393F}$, $Mdm2^{S394A}$, and $Mdm2^{Y393F/S394A}$ mice untreated or 8 h following 5 Gy IR ($n = 3$–6, ± SEM). $^*P < 0.05$, $^{**}P < 0.01$ (Student's *t* tests).

staining followed by flow cytometry of $Mdm2^{Y393F/S394A}$ thymi relative to those seen in $Mdm2^{S394A}$ thymi (Fig. S5 *C* and *D*).

Finally, we examined whether the radioresistant phenotypes observed in $Mdm2^{Y393F}$ and $Mdm2^{S394A}$ mice were exacerbated in $Mdm2^{Y393F/S394A}$ mice. $Mdm2^{S394A}$ and $Mdm2^{Y393F/S394A}$ mice were exposed to 9 Gy whole-body IR (as used for $Mdm2^{Y393F}$ mice) and monitored for signs of morbidity (Fig. 4*F*). No significant difference in survival was observed between $Mdm2^{S394A}$ and $Mdm2^{Y393F/S394A}$ mice at this dose, with 82% of $Mdm2^{S394A}$ mice and 69% of $Mdm2^{Y393F/S394A}$ mice surviving at 4 wk, respectively. However, both genotypes are significantly more radioresistant than $Mdm2^{Y393F}$ mice, which are themselves significantly more radioresistant than WT mice at this dose. Thus, radioresistance resulting from the loss of either Mdm2 Tyr393 phosphorylation by c-Abl or Mdm2 Ser394 phosphorylation by ATM is not increased by mutation of both phospho-target residues. Accordingly, IR-induced expression levels of p53-target genes in irradiated bone marrow of $Mdm2^{S394A}$ and $Mdm2^{Y393F/S394A}$ mice are similarly reduced (Fig. S6*A*). The equivalent deficiency in the p53 response in $Mdm2^{S394A}$ and $Mdm2^{Y393F/S394A}$ bone marrow follows with comparably increased numbers of L^-SK HSPCs surviving in $Mdm2^{Y393F/S394A}$ bone marrow following IR (Fig. 4*G*). Furthermore, bone marrow cells from $Mdm2^{Y393F/S394A}$ or $Mdm2^{S394A}$ mice exhibit similar hematopoietic repopulating abilities in vivo (Fig. S6*B*). As was observed with $Mdm2^{Y393F}$ and $Mdm2^{S394A}$ mice, no differences were seen in the number of lineage-defined or L^-S^-K hematopoietic cells (Fig. S6 *C* and *D*).

Discussion

These findings provide further evidence of the significance of phosphorylation of Mdm2 by DNA damage-activated kinases in regulating p53-dependent organismal responses. $Mdm2^{Y393F}$ mice are viable and display no developmental defects, yet they are significantly more prone to developing spontaneous tumors over their lifespan (Fig. 1*B*). The spontaneous tumors arising in $Mdm2^{Y393F}$ mice are primarily hematopoietic in nature and led us to examine whether Mdm2 Tyr393 phosphorylation impacted oncogene-induced tumorigenesis using the *Eμ-Myc* allele. Indeed, *Eμ-Myc;*$Mdm2^{Y393F}$ mice developed tumors at a significantly accelerated rate (Fig. 1*F*).

The increased spontaneous tumorigenesis rates and accelerated B-cell lymphomagenesis are a likely result of reduced p53 activity in $Mdm2^{Y393F}$ and *Eμ-Myc;*$Mdm2^{Y393F}$ mice, as p53-dependent apoptosis and senescence have been shown to inhibit spontaneous tumorigenesis and B-cell tumors induced by aberrant Myc activity (24, 30–32). However, we observed no defects in p53-dependent apoptosis in spleens or thymi of $Mdm2^{Y393F}$ mice following IR, or p53-dependent growth arrest in MEFs treated with IR or doxorubicin (Fig. 2 and Fig. S2). It is conceivable that Mdm2 phosphorylation by c-Abl can regulate p53 tumor suppressing effects other than apoptosis or growth arrest, and/or that subtle differences in these p53 functions in $Mdm2^{Y393F}$ mice are not detectable by examining the effects of acute damage on p53 tumor suppression. Furthermore, it is possible that additional c-Abl target residues on Mdm2 can compensate for the loss of Mdm2 Tyr393 phosphorylation (12, 13).

Seemingly incongruously, $Mdm2^{Y393F}$ mice are resistant to threshold-lethal doses of radiation (Fig. 3*A*). This radioresistance parallels our previous observations with $Mdm2^{S394A}$ mice, which display profound defects in p53-dependent apoptosis and tissues. HSPC or bone marrow cells from both mutants display improved repopulating functions following IR exposure, albeit to a greater extent in $Mdm2^{S394A}$ mice (Fig. 3*D*). In keeping with this difference, HSPCs in $Mdm2^{S394A}$ bone marrow display a significant survival advantage following IR, whereas $Mdm2^{Y393F}$ HSPCs display only a marginal increase in survival after DNA damage. However, the slight increase in the survival of $Mdm2^{Y393F}$ HSPCs manifests increased radioresistance in $Mdm2^{Y393F}$ mice relative to WT mice.

The generation of $Mdm2^{Y393F/S394A}$ mice allowed us to examine whether the common effects of Mdm2 Tyr393 phosphorylation by c-Abl and Mdm2 Ser394 phosphorylation by ATM are additive or redundant. We observed no additive or synergistic effects of the loss of both phosphorylation events on the incidence of spontaneous tumorigenesis, with $Mdm2^{Y393F/S394A}$ mice developing spontaneous tumors at a frequency and latency that nearly overlaps what we have reported with $Mdm2^{S394A}$ mice (Fig. 4*B*). Similarly, we observed no additive effects on radioresistance, with $Mdm2^{Y393F/S394A}$ and $Mdm2^{S394A}$ mice displaying comparable survival, HSPC numbers, and bone marrow reconstitution following whole-body IR (Fig. 4 *F* and *G* and Fig. S6). Hence, there is an apparent redundancy of the shared phenotypes between $Mdm2^{Y393F}$ and $Mdm2^{S394A}$ mice, with tumorigenesis and radioresistance in $Mdm2^{Y393F/S394A}$ mice never exceeding that observed in $Mdm2^{S394A}$ mice. This may reflect the proposed interdependence of c-Abl and ATM for their respective activities (16, 33, 34). However, ATM phosphorylation of Mdm2 Ser394 clearly has a predominant effect on Mdm2-p53 signaling and p53 functions, relative to the effects induced by c-Abl phosphorylation of Mdm2 Tyr393.

Methods

Mice and Animal Studies. All animals described in this study were on a C57BL/6 background. Mice and cells were irradiated with a cesium-137 source (Gammacell 40). The generation of $Mdm2^{S394A}$ mice has been previously described (11). *Eμ-Myc* mice were a gift from Christine Eischen, Vanderbilt University, Nashville. TN. A detailed description of the generation and genotyping of $Mdm2^{Y393F}$ and $Mdm2^{Y393F/S394A}$ mice is provided in *SI Methods*. All animals used in this study were maintained and assayed in accordance with federal guidelines and those established by the Institutional Animal Care and Use Committee at the University of Massachusetts Medical School (UMMS).

Immunoblotting. Tissues and cells were lysed in Nonidet P-40 lysis buffer supplemented with protease and phosphatase inhibitors. A detailed description of the methods used, including antibodies and clones, is provided in *SI Methods*.

Gene Expression Analysis and Sequencing. Total RNA was isolated from tissues by RNeasy Mini Kit (Qiagen) and cDNA synthesized by the SuperScript III First Strand Synthesis System (Invitrogen). qPCR was performed using SYBR Select Master Mix (Applied Biosystems) in conjunction with a 7300 Real-Time PCR System (Applied Biosystems). A detailed description of the methods used for qPCR and sequencing is provided in *SI Methods*.

Histopathology. Tissue samples were fixed in 10% (vol/vol) formalin for 24 h. The UMMS Morphology Core Laboratory performed embedding, sectioning, and staining. TUNEL staining was performed using the In Situ Cell Death Detection Kit, POD (Roche) according to manufacturer's instructions. Immunohistochemistry was performed with antibodies specific for B220 (550286; BD Pharmingen) and CD3 (A0452; Dako). Naphthol chloroacetate esterase staining was performed to detect cells with myeloid differentiation. Stained tissue was analyzed using an Olympus CX41 microscope fitted with a PixeLINK camera and software.

Bone Marrow Analysis. Total bone marrow from both hind limbs was harvested, RBCs were lysed, and single-cell suspensions were stained with cell-surface antibodies for Gr-1, CD11B, CD3, and B220. For LSK analysis, bone marrow cells were stained with a biotin lineage mixture and antibodies for Sca-1, c-Kit, CD34, and Flk2. All samples were run on a BD LSRII flow cytometer (BD Biosciences) and analyzed using FlowJo software (Tree Star). A complete list of antibodies including clone numbers is given in Table S1.

Statistical Analysis. Statistical analyses were performed using GraphPad Prism software, version 6.0d. Kaplan–Meier survival curves were analyzed by log-rank test. A P value of <0.05 was considered statistically significant for Student t tests.

ACKNOWLEDGMENTS. This research was supported by NIH Grants R01-CA077735 (to S.N.J.) and R01-CA096899 (to M.A.K.). J.E.R. was supported by Postdoctoral Fellowship 125087-PF-13-247-01-LIB from the American Cancer Society.

1. Vogelstein B, Lane D, Levine AJ (2000) Surfing the p53 network. *Nature* 408(6810):307–310.
2. Li T, et al. (2012) Tumor suppression in the absence of p53-mediated cell-cycle arrest, apoptosis, and senescence. *Cell* 149(6):1269–1283.
3. Valente LJ, et al. (2013) p53 efficiently suppresses tumor development in the complete absence of its cell-cycle inhibitory and proapoptotic effectors p21, Puma, and Noxa. *Cell Reports* 3(5):1339–1345.
4. Jackson SP, Bartek J (2009) The DNA-damage response in human biology and disease. *Nature* 461(7267):1071–1078.
5. Ciccia A, Elledge SJ (2010) The DNA damage response: Making it safe to play with knives. *Mol Cell* 40(2):179–204.
6. Shieh S-Y, Ikeda M, Taya Y, Prives C (1997) DNA damage-induced phosphorylation of p53 alleviates inhibition by MDM2. *Cell* 91(3):325–334.
7. Shieh S-Y, Ahn J, Tamai K, Taya Y, Prives C (2000) The human homologs of checkpoint kinases Chk1 and Cds1 (Chk2) phosphorylate p53 at multiple DNA damage-inducible sites. *Genes Dev* 14(3):289–300.
8. Maya R, et al. (2001) ATM-dependent phosphorylation of Mdm2 on serine 395: Role in p53 activation by DNA damage. *Genes Dev* 15(9):1067–1077.
9. Pereg Y, et al. (2005) Phosphorylation of Hdmx mediates its Hdm2- and ATM-dependent degradation in response to DNA damage. *Proc Natl Acad Sci USA* 102(14):5056–5061.
10. Chen L, Gilkes DM, Pan Y, Lane WS, Chen J (2005) ATM and Chk2-dependent phosphorylation of MDMX contribute to p53 activation after DNA damage. *EMBO J* 24(19):3411–3422.
11. Gannon HS, Woda BA, Jones SN (2012) ATM phosphorylation of Mdm2 Ser394 regulates the amplitude and duration of the DNA damage response in mice. *Cancer Cell* 21(5):668–679.
12. Goldberg Z, et al. (2002) Tyrosine phosphorylation of Mdm2 by c-Abl: Implications for p53 regulation. *EMBO J* 21(14):3715–3727.
13. Dias SS, Milne DM, Meek DW (2006) c-Abl phosphorylates Hdm2 at tyrosine 276 in response to DNA damage and regulates interaction with ARF. *Oncogene* 25(50):6666–6671.
14. Kharbanda S, et al. (1995) Activation of the c-Abl tyrosine kinase in the stress response to DNA-damaging agents. *Nature* 376(6543):785–788.
15. Liu Z-G, et al. (1996) Three distinct signalling responses by murine fibroblasts to genotoxic stress. *Nature* 384(6606):273–276.
16. Wang X, et al. (2011) A positive role for c-Abl in Atm and Atr activation in DNA damage response. *Cell Death Differ* 18(1):5–15.
17. Wen ST, Jackson PK, Van Etten RA (1996) The cytostatic function of c-Abl is controlled by multiple nuclear localization signals and requires the p53 and Rb tumor suppressor gene products. *EMBO J* 15(7):1583–1595.
18. Yuan Z-M, et al. (1997) Regulation of DNA damage-induced apoptosis by the c-Abl tyrosine kinase. *Proc Natl Acad Sci USA* 94(4):1437–1440.
19. Sionov RV, et al. (1999) c-Abl neutralizes the inhibitory effect of Mdm2 on p53. *J Biol Chem* 274(13):8371–8374.
20. Sionov RV, et al. (2001) c-Abl regulates p53 levels under normal and stress conditions by preventing its nuclear export and ubiquitination. *Mol Cell Biol* 21(17):5869–5878.
21. Waning DL, Lehman JA, Batuello CN, Mayo LD (2011) c-Abl phosphorylation of Mdm2 facilitates Mdm2-Mdmx complex formation. *J Biol Chem* 286(1):216–222.
22. O'Gorman S, Dagenais NA, Qian M, Marchuk Y (1997) Protamine-Cre recombinase transgenes efficiently recombine target sequences in the male germ line of mice, but not in embryonic stem cells. *Proc Natl Acad Sci USA* 94(26):14602–14607.
23. Adams JM, et al. (1985) The c-myc oncogene driven by immunoglobulin enhancers induces lymphoid malignancy in transgenic mice. *Nature* 318(6046):533–538.
24. Eischen CM, Weber JD, Roussel MF, Sherr CJ, Cleveland JL (1999) Disruption of the ARF-Mdm2-p53 tumor suppressor pathway in Myc-induced lymphomagenesis. *Genes Dev* 13(20):2658–2669.
25. Barilà D, et al. (2003) Caspase-dependent cleavage of c-Abl contributes to apoptosis. *Mol Cell Biol* 23(8):2790–2799.
26. Machuy N, Rajalingam K, Rudel T (2004) Requirement of caspase-mediated cleavage of c-Abl during stress-induced apoptosis. *Cell Death Differ* 11(3):290–300.
27. Pant V, et al. (2013) The p53-Mdm2 feedback loop protects against DNA damage by inhibiting p53 activity but is dispensable for p53 stability, development, and longevity. *Genes Dev* 27(17):1857–1867.
28. Gudkov AV, Komarova EA (2003) The role of p53 in determining sensitivity to radiotherapy. *Nat Rev Cancer* 3(2):117–129.
29. Komarova EA, et al. (2004) Dual effect of p53 on radiation sensitivity in vivo: p53 promotes hematopoietic injury, but protects from gastro-intestinal syndrome in mice. *Oncogene* 23(19):3265–3271.
30. Eischen CM, Roussel MF, Korsmeyer SJ, Cleveland JL (2001) Bax loss impairs Myc-induced apoptosis and circumvents the selection of p53 mutations during Myc-mediated lymphomagenesis. *Mol Cell Biol* 21(22):7653–7662.
31. Schmitt CA, et al. (2002) Dissecting p53 tumor suppressor functions in vivo. *Cancer Cell* 1(3):289–298.
32. Post SM, et al. (2010) p53-dependent senescence delays Emu-myc-induced B-cell lymphomagenesis. *Oncogene* 29(9):1260–1269.
33. Baskaran R, et al. (1997) Ataxia telangiectasia mutant protein activates c-Abl tyrosine kinase in response to ionizing radiation. *Nature* 387(6632):516–519.
34. Shafman T, et al. (1997) Interaction between ATM protein and c-Abl in response to DNA damage. *Nature* 387(6632):520–523.